



# The Effect of Spacer Orientations on Temperature Polarization in a Direct Contact Membrane Distillation Process Using 3-d CFD Modeling

S. M. F. Hasani<sup>1</sup> · A. S. Sowayan<sup>1</sup> · M. Shakaib<sup>2</sup>

Received: 14 February 2019 / Accepted: 1 August 2019 / Published online: 26 August 2019  
© King Fahd University of Petroleum & Minerals 2019

## Abstract

Membrane distillation is an emerging technology that uses hydrophobic membranes to separate nonvolatile solids from liquids. The vapor pressure gradient between the feed and the permeate sides drives the process. Low-grade thermal energy is used to heat feed water and create a pressure gradient. A large vapor pressure gradient across the membrane surfaces results in high permeation rates. The feed spacer is an important element of the membrane module that forms channels for feed and permeate flow. A good feed spacer design helps improve permeation. In this paper, 3-d CFD simulations are carried out for spacer-filled channels, and the effect of inlet velocity, filament orientation and spacing on heat transfer is studied. Temperature polarization is used as the parameter for heat transfer performance evaluation. Shear stress and temperature polarization index have been calculated for different spacer orientations in a direct contact membrane distillation process. The results show a major influence of the studied parameters on temperature polarization and shear stress. A comparison of 2-d and 3-d analyses reveals that the average shear stress in the two approaches is nearly the same, but the standard deviation of shear stress is lower for the 2-d case. Similarly, the average value and the standard deviation of temperature polarization index are lower than those obtained in the 3-d analysis. The findings also show that for staggered axial filaments, the temperature polarization index distribution is more uniform suggesting that such orientations are more suitable for enhancing heat transfer in a membrane distillation process.

**Keywords** CFD simulation · Feed spacer · Membrane distillation · Shear stress · Temperature polarization

## List of Symbols

$C_p$  Specific heat (J/kg K)  
 $d_f$  Filament diameter (m)  
 $d_h$  Hydraulic diameter (m)  
 $h$   $\left( = \frac{q_w}{T_h - T_{hm}} = \frac{q_w}{T_{cm} - T_c} \right) \equiv$  heat transfer coefficient (W/m<sup>2</sup> K)  
 $h_{ch}$  Channel height (m)  
 $k$  Thermal conductivity (W/m K)  
 $L$  Channel length (m)  
 $l_m$  Mesh length/filament spacing (m)  
 $Nu$  Nusselt number  $\left( = \frac{hd_h}{k} \right)$

$Pr$  Prandtl number  $\left( = \frac{\mu C_p}{k} \right)$   
 $q_w$  Heat flux (W/m<sup>2</sup>)  
 $Re$  Reynolds number  $\left( = \frac{\rho v d_h}{\mu} \right)$   
 $u_{av}$  Average velocity (m/s)  
 $T_c$  Inlet temperature of cold fluid (K)  
 $T_{cm}$  Temperature at membrane surface in cold channel (K)  
 $T_h$  Inlet temperature of hot fluid (K)  
 $T_{hm}$  Temperature at membrane surface in hot channel (K)  
 $\rho$  Density (kg/m<sup>3</sup>)  
 $\tau_{av}$  Average value of shear stress  
 $\tau_{sd}$  Standard deviation of shear stress  
 $\Phi$  Temperature polarization index  
 $\phi_{av}$  Average value of temperature polarization index  
 $\phi_{sd}$  Standard deviation of temperature polarization index  
 $\mu$  Viscosity (kg/m s)  
 $\varepsilon$  Voidage of feed or permeate channel  
 $\theta$  Flow attack angle

✉ S. M. F. Hasani  
smhasani@imamu.edu.sa

<sup>1</sup> Department of Mechanical Engineering, Al Imam Mohammad Ibn Saud Islamic University, Riyadh, Saudi Arabia

<sup>2</sup> Department of Mechanical Engineering, NED University of Engineering and Technology, Karachi, Pakistan



## 1 Introduction

Cross-flow membrane techniques are predominantly used in a variety of fluid separation and treatment applications. A membrane process that has regained researchers' attention in recent years is membrane distillation (MD). It is a process in which nonvolatile solids and in some cases volatile substances are separated from the water as it passes through a hydrophobic membrane. The temperature/vapor pressure gradient across the membrane is the driving force for separation. The process requires low operating temperatures, and the operating pressures are lower than those encountered in other membrane processes, and it has a high salt rejection rate. Current research trends are in the direction of making this technology commercially viable to compete with existing membrane separation technologies. One possible way of achieving this is through the improvement in the membrane module design.

Spiral-wound type modules are widely used with such systems as they offer a larger surface area to volume ratio. A schematic of the module is shown in Fig. 1.

Net-type spacers in the feed and permeate channels are important components of this module. The spacer in the feed channel keeps the wound membrane layers apart, provide height to the flow channels, promote turbulence and gives strength and stability to the module. A blown-up view of spacer filament layout across the membrane is shown in Fig. 2.

The permeation of vapor through the membrane depends on various factors such as membrane permeability and the heat transferred across the membrane. This process of heat transfer is governed by the phenomenon of temperature polarization. A temperature polarization index is used in the paper which is defined as the ratio of the bulk stream temperature difference to the temperature difference across the membrane surfaces in the two channels. For better heat transfer and higher permeation through the membrane, the

**Fig. 1** Spiral-wound membrane distillation module (Courtesy: GE Osmonics Inc.)

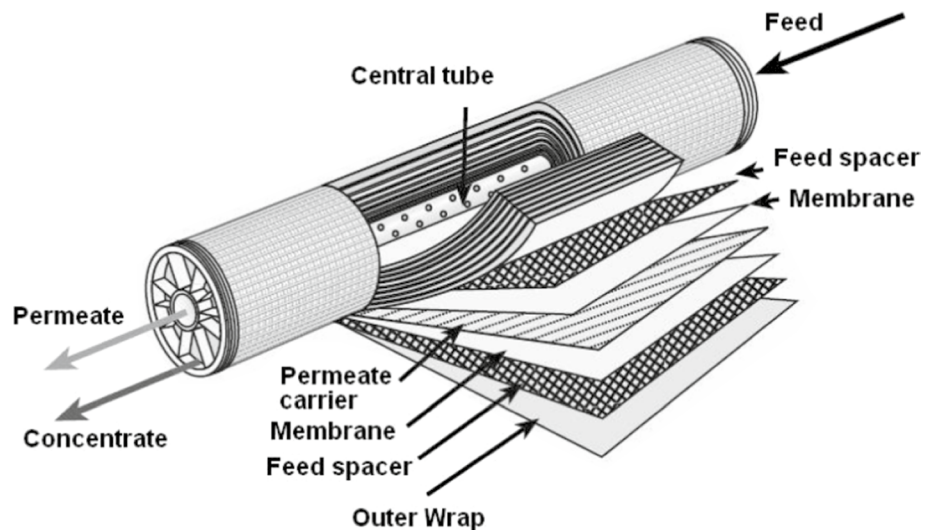
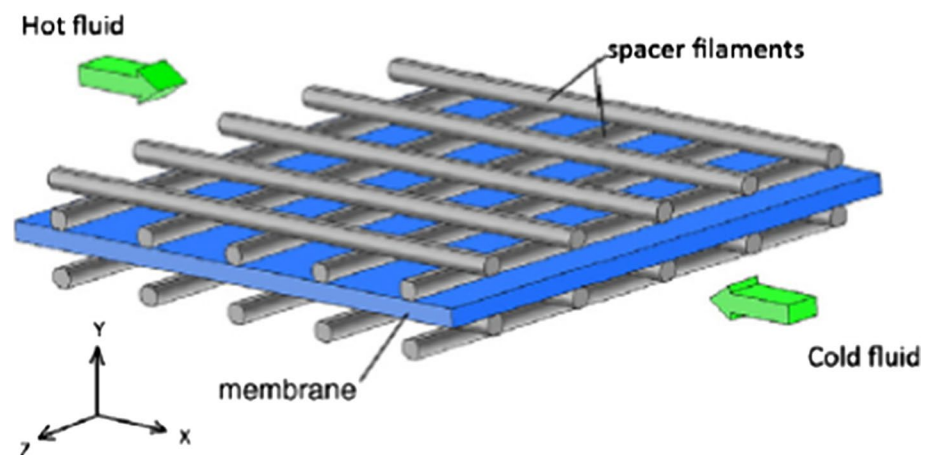


**Fig. 2** Spacer-filled membrane distillation channels [1]

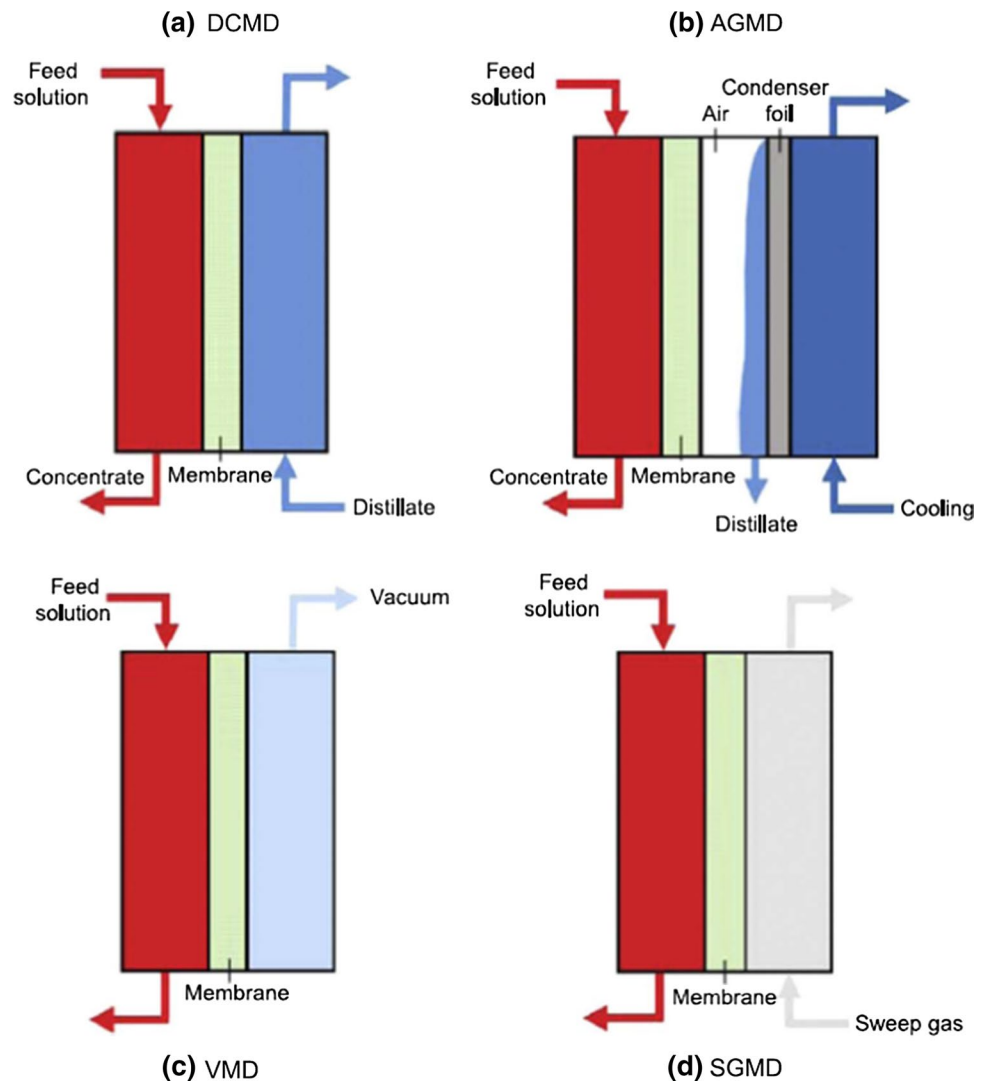


temperature polarization index has to be low. The presence of spacer disrupts the concentration and thermal boundary layers, creates turbulence and increases the permeation rate, while on the other hand they also form localized stagnant zones behind the spacer filaments. These stagnant zones increase the temperature polarization index and decrease the driving force for permeation. Therefore, the spacer orientation (alignment and positioning of the spacer filaments with respect to the flow direction in the feed and the permeate channels) and filament spacing are important parameters that affect temperature polarization and hence the permeation rate. The feed channel contains saline fluid, while the permeate channel contains the distillate that is evaporated through the membrane and condensed on the permeate side. The condensing surface may be in direct contact (DCMD) with the evaporated vapors, or it is separated by an air gap (AGMD), or a sweeping gas (SGMD) or through a vacuum (VMD) depending on the type of MD configuration employed. These various MD vapor condensation mechanisms are shown in

Fig. 3. Among the different MD configurations/processes, the direct contact membrane distillation (DCMD) is the most widely used and studied process as it requires the least equipment, is simple to operate and is suited for some basic applications such as water desalination and fruit juice concentration. Gonzalez et al. [2] in a recent paper provided a comprehensive review of the MD technology in the last thirty years. They noted renewed interest in the technology and attributed it to its sustainable nature and the ease of energization using renewable energies and waste heat. Computational fluid dynamics (CFD) technique to model MD processes has been found as a powerful tool. Shirazi et al. [3] reviewed the CFD studies applied to model MD processes. Acknowledging the power of CFD as a modeling tool, they highlighted areas in MD research where CFD could be used.

In this paper, a three-dimensional CFD model is applied to model a DCMD process. The DCMD offers several advantages in niche areas, including the processing of high osmotic pressure feeds and at extremes of pH and for

**Fig. 3** Membrane distillation vapor condensation mechanisms [2]



small-scale remote systems using solar or waste heat. It uses feed fluid at a high temperature and concentration that flows parallel to the membrane on one side while the product fluid with lower temperature and concentration flows on the other side of the membrane usually in the opposite (counter flow) direction. During the process, a small amount of feed at higher temperature permeates through the membrane in the vapor form due to the temperature gradient and mixes with the fluid on the other side. A characteristic or a limitation of the DCMD process is that the difference of temperatures on the two sides of the membrane surface is lower than the difference of the bulk temperatures of the hot and cold fluids. This is termed as temperature polarization which reduces the thermal driving force and thus the water permeation rates. Net-type spacers are commonly employed in membrane modules to promote the mixing of fluid near the membrane surface with the bulk fluid in order to reduce the temperature polarization phenomenon. Properly designed spacers can minimize the temperature polarization phenomenon.

Several papers have been published that study the temperature polarization and the effect of spacer geometry and orientation on the performance of the membrane distillation process. Phattaranawik et al. [4] had shown that the presence of spacers enhances both the mass and heat transfer in a DCMD process. In another paper, Phattaranawik et al. [5] showed that temperature polarization could be reduced by 30–40% by choosing different geometries of the spacers. Martínez et al. [6] and Martínez and Rodríguez-Maroto [7] studied two basic separator type configurations: open flow separators and screen separators. The use of screen separator (or spacer) resulted in the formation of eddies and wakes, which decreased temperature polarization and offered as a better option for use in MD processes as compared to the open type. In another work, Martínez and Gonzalez [8] investigated temperature and concentration patterns in an MD process and found that the permeate flux reduced due to temperature polarization while the effect of concentration polarization was less significant. Chernyshov et al. [9] studied the effect of spacers for an air gap membrane distillation process and observed that the permeate flux with spacers is about 2.5 times higher than the flux in the empty channel. Xu et al. [10] simulated the temperature profiles for air gap membrane distillation and proved that the temperature polarization phenomenon can be reduced by increasing feed Reynolds number. Alkhalabi and Lior [11] performed simulations for three different spacer arrangements namely: zigzag spacer, non-central suspended and central suspended. The three arrangements were examined based on spacer effectiveness. The central suspended spacer showed the best performance. CFD studies were performed for commercial and custom-made spacer geometries by Cipollina et al. [12, 13]. Recently, Jangwon et al. [14] performed a spacer optimization study for a DCMD process. They considered

spacers of different shapes, configurations, diameters and spacing and concluded that symmetrical circular-zigzag spacer performed best and produced vapor flux 26% higher than the empty channel. All these studies showed reduced temperature polarization due to the presence of transverse filaments. Al-Sharif et al. [15] used an open-source CFD code to model fluid flow and heat transfer in spacer-filled membrane distillation channels. A 3-layer spacer was found to have the lowest pressure drop and symmetrical temperature profile in the membrane channel. Yu et al. [16] found that the temperature polarization decreases with the increase in operating temperature. Chang et al. [17] conducted a 3-d numerical study for heat and mass transfer in a spacer-filled MD module considering its entire length. They only considered laminar flow for which the Nusselt numbers obtained through CFD analysis were found to be higher than the published experimental results. In another comprehensive CFD study, Katsandri [18] performed a theoretical analysis of a spacer-filled flat plate membrane distillation module and validated the results through his experimental work [19]. The study considered permeation through the membrane but due to the complexities associated with numerical modeling only laminar flow was considered. In our prior work [1, 20], we presented results of two-dimensional (2-d) analysis and showed a significant effect of filament spacing and orientation on fluid flow and heat transfer in membrane distillation channels. The 2-d modeling technique requires relatively less computational space and time to yield results. However, through 2-d approach, the effect of one set of filament (e.g., transverse filament) can be studied and the presence of another set of filament (which is axial in the present study) is ignored. In spacer-filled channels, both sets of filaments can affect hydrodynamics, distribution of foulants and thus the membrane performance as known from experimental studies [21, 22]. This work is an extension of our previous study, and it includes three-dimensional (3-d) simulations. The effect of the both sets of filaments along with the arrangement of these filaments (in-line or staggered) is examined. The paper includes the calculation of heat transfer rates and temperature polarization in membrane distillation modules. The differences of results of 3-d with 2-d ones are discussed and suitable orientation/placement of spacers in membrane channel is identified. The feed velocities for which the flow turned turbulent are also considered in the analysis.

## 2 The Computational Model

The MD modules use net-type spacers that usually consist of two layers/sets of filaments, one overlaying upon the other. In flow-aligned spacers, the filaments are perpendicular to each other, the filament parallel to the flow direction is called axial (or longitudinal) filament while the one perpendicular

to it is referred to as the transverse (or cross) filament. Santos et al. [23] showed that the transverse filaments play a more significant role in determining the flow characteristics. For this reason, many studies modeled the fluid flow in membrane channels as two-dimensional and considered only the effect of the transverse filaments. In our prior work [1], the effect of spacer orientation on temperature polarization in MD channels was studied and it was found that the orientations in which transverse filaments did not touch the membrane were more suitable for adoption as they resulted in lower temperature polarization index ( $\phi$ ) values. In this paper, 3-d modeling is carried out which included the effect of axial filaments. The results of the earlier 2-d analysis have been used for comparison with this 3-d modeling work. Four different spacer orientations have been used for the 3-d model, and they are compared with two orientations of the previous 2-d analysis. Table 1 describes the nomenclature used in this paper for all spacer orientations, while Fig. 4 describes the computational domains used in the analysis.

Since the 2-d analysis does not include axial filaments, its domain consists of multiple transverse filaments, whereas the 3-d domain comprises of a single axial and multiple transverse filaments. The spacers used in previous experimental studies and commercial membrane modules have thickness/height in the range 0.2–2 mm and filament spacing (per unit spacer height) between 2 and 8 [5, 6, 24]. In the present work, typical dimensions of spacer and membrane thickness are used. The thickness of spacer (or height of channel), thus, for both the feed and the permeate channels is 1 mm and the membrane thickness is 0.2 mm. The spacer filament height is 0.5 mm and spacing ( $l_m$ ) between two successive filaments is varied between 3 and 4.5 mm. The notations of Table 1 for different spacer configurations are followed by numbers 30 or 45 to indicate the spacing. For example, 2DC1-30 means a 2-d in-line spacer with a spacing of 3 mm and 3DC4-45 refers to a 3-d spacer with staggered filaments and a spacing of 4.5 mm.

Velocities are specified at the inlets of the feed and permeate channels, while pressure boundary conditions are used at the outlets. For 3-d simulations, flow symmetry is employed along the axial filaments. The flow and temperature profiles within the feed flow channel depend on the permeation rate through the membrane. As the permeability of membrane

increases, the flow patterns and other parameters change [25]. The permeation rate, however, in the MD process is very low when compared to the feed flow rate. In a typical MD unit, product/permeate flux is around 75 kg/m<sup>2</sup> h [26] which means permeate velocity of  $2 \times 10^{-5}$  m/s. When permeate flow velocities are lower ( $\approx 2 \times 10^{-5}$  m/s), the parameters of flow and heat transfer such as heat transfer coefficient or temperature polarization are approximately the same as calculated using wall boundary condition for membrane [20, 25]. The membrane under conditions of low permeation rates, thus, can be considered impermeable with negligible error. The two fluids flow in a counterflow direction. The temperature of hot fluid is 330 K, whereas the cold fluid temperature is set at 300 K. The feed fluid is water with constant density and thermal conductivity, but viscosity varies with temperature. The fluid inlet velocity is varied from 0.05 to 0.2 m/s. A portion of the computational grid for 2-d and 3-d simulations is shown in Fig. 5. There are about 25,000 cells in the 2-d mesh and 1,000,000 cells in the 3-d mesh. Mesh-independence tests are conducted to determine the adequacy of the computational meshes. ANSYS FLUENT 12 is used to solve three-dimensional continuity, momentum and energy equations [27, 28]. The flow becomes turbulent for velocities greater than 0.14 m/s, and the Spalart–Allmaras model [27] is used for turbulent flow modeling. The momentum equations are discretized using the QUICK scheme, while power law scheme is used for the energy equation and the turbulence model [27, 28]. The spacer orientation effectiveness is determined based on the obtained temperature polarization index ( $\phi$ ) values defined as:

$$\phi = \frac{T_h - T_c}{T_{hm} - T_{cm}} \tag{1}$$

where  $T_h$  and  $T_c$  are the inlet temperatures of hot and cold fluids, respectively.  $T_{hm}$  and  $T_{cm}$  are the membrane surface temperatures at the hot (top) and cold (bottom) sides. A smaller value of  $\phi$  is desirable.

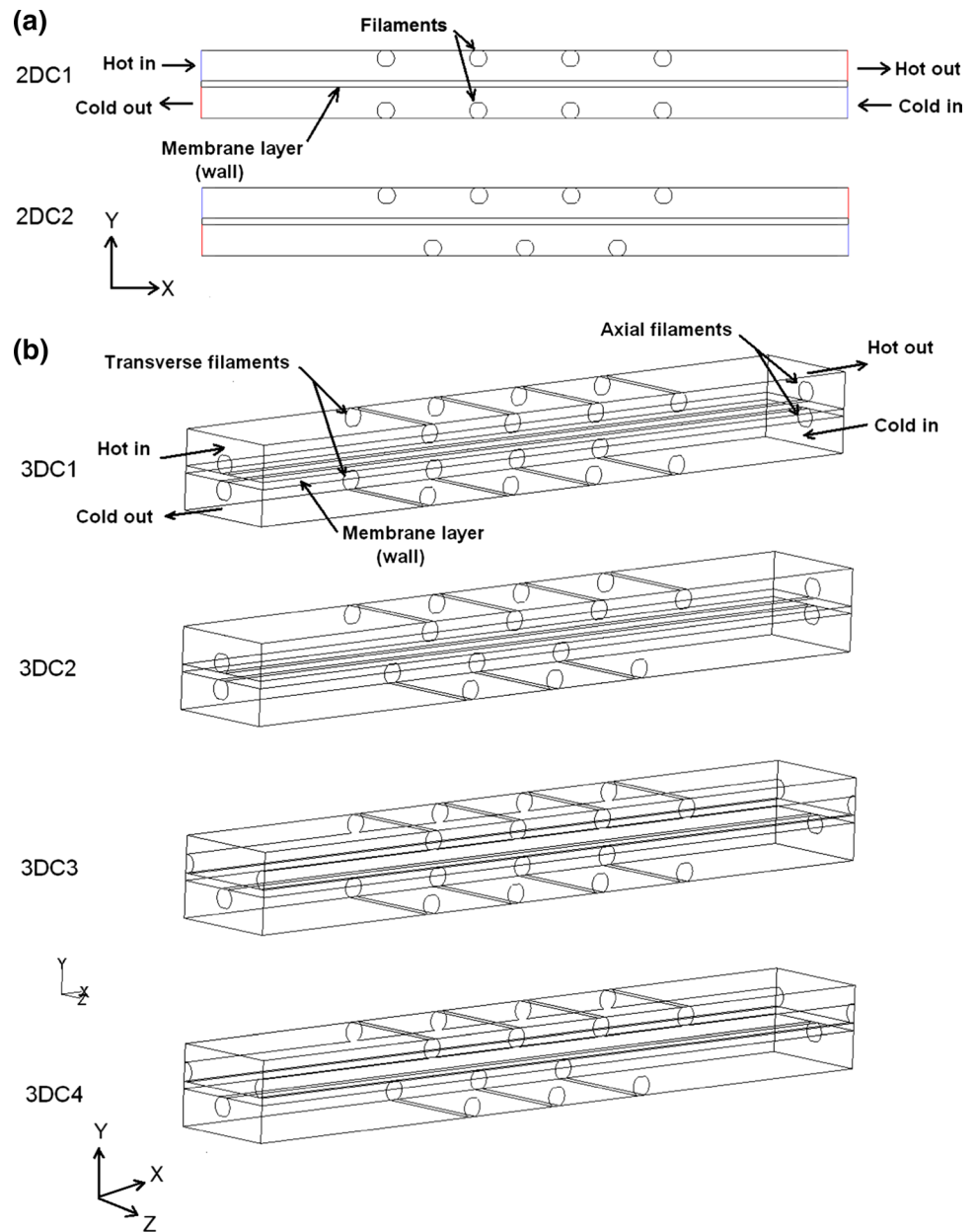
Nusselt number ( $Nu$ ) is calculated for comparing present results with previous experimental studies. The following relation is used:

$$Nu = \frac{hd_h}{k} \tag{2}$$

**Table 1** Spacer orientation nomenclature

Model type	Description	Notation
2-d	Filaments (in transverse direction) are in-line in the two channels	2DC1
2-d	Filaments in both (hot and cold) channels are staggered	2DC2
3-d	Transverse and axial filaments are in-line in the two channels	3DC1
3-d	Transverse filaments are staggered but axial filaments are in-line	3DC2
3-d	Transverse filaments are in-line but axial filaments are staggered	3DC3
3-d	Both transverse and axial filaments are staggered	3DC4

**Fig. 4** Computational domains for **a** 2-d and **b** 3-d spacer orientations



In the above equation,  $h$  is heat transfer coefficient,  $d_h$  is hydraulic diameter and  $k$  is thermal conductivity. The comparison is done with the experimental correlations/Eqs. (3) and (4) which are suggested in the literature for spacer-filled channels.

$$Nu = \alpha \left[ 4.36 + \frac{0.036 Re Pr (d_h/L)}{1 + 0.0011 (Re Pr (d_h/L))^{0.8}} \right] \quad (3)$$

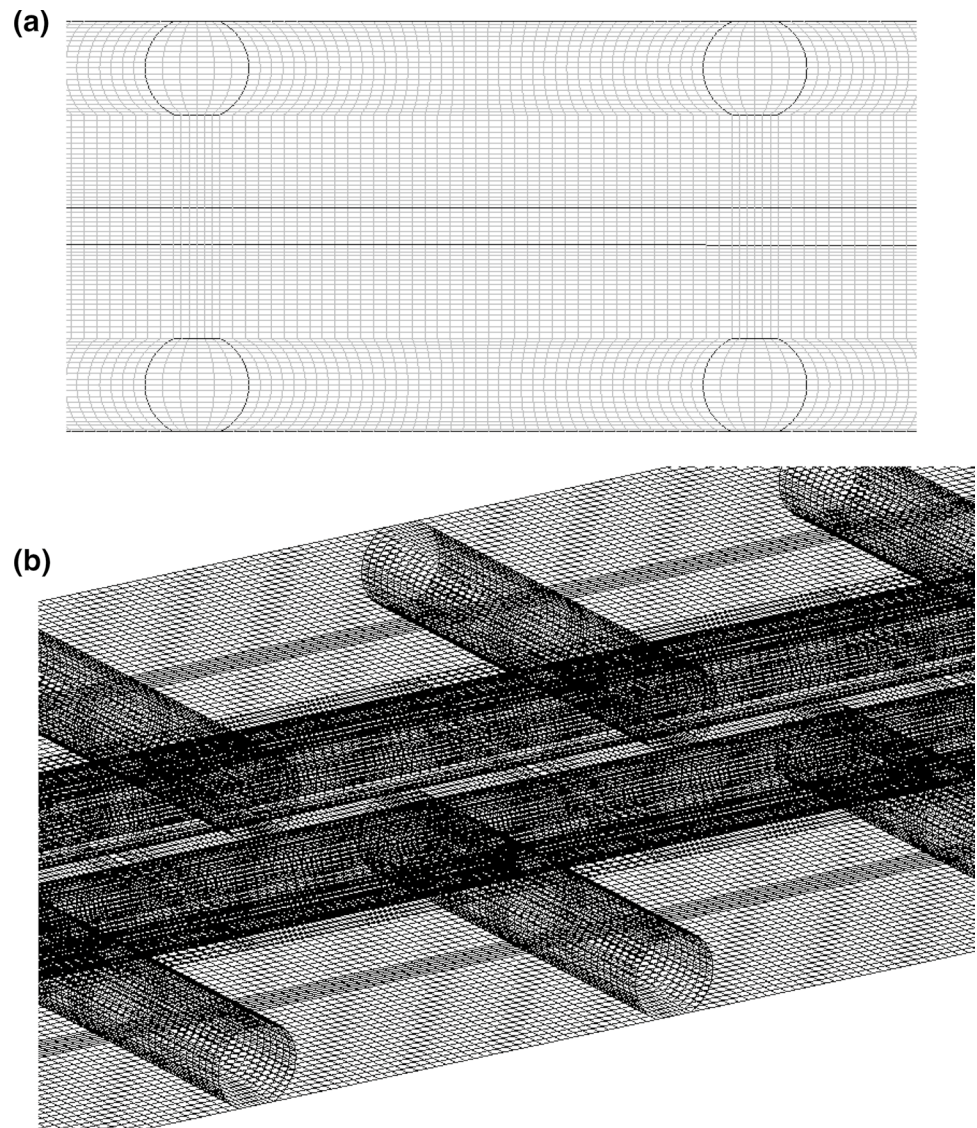
where

$$\alpha = 1.88 \left( \frac{d_f}{h_{ch}} \right)^{-0.039} (\sin \theta)^{1.33} \times \exp \left( -4.05 \left( \left[ \ln \left( \frac{\epsilon}{\epsilon_m} \right) \right]^2 \right) \right)$$

$$Nu = 0.664 Re^{0.5} Pr^{0.33} \left( \frac{d_h}{l_m} \right)^{0.5} \quad (4)$$

Equation (3) was specifically developed for heat transfer in a spacer-filled MD channel [5], while Eq. (4) generally known as the Grober equation was derived for mass transfer [24] in spacer-filled ultrafiltration channel. Equation (4) can be used for heat transfer because of the similarity that exists between heat and mass transfer [4].

**Fig. 5** Computational grid for **a** 2DC1-30 **b** 3DC1-30



### 3 Results and Discussion

The velocity and temperature profiles have been obtained for the various configurations of Table 1 with variable filament spacing. Figures 6a–f shows these profiles for the in-line 3-d configuration 3DC1-30, while Fig. 6g, h is for the corresponding 2-d geometry 2DC1-30. For the 3-d case, sectional profiles are shown at three vertical planes P1 (a, b), P2 (c, d) and P3 (e, f) at dimensionless distance  $z=0.12, 0.3$  and  $0.5$  from the axial filament. (The  $z$  dimension is non-dimensionalized using the filament spacing  $l_m$ .) The 2-d velocity and temperature fields are shown in Fig. 6g, h.

In the hot or the cold channels, the velocity contours of Fig. 6a, c, e, g show two distinct regions: Region I which lies between the membrane surface and the filaments has higher velocity magnitudes and region II, which is adjacent to the filaments (on right side of filaments in hot feed channel or on

left side in permeate channel) where velocities are smaller. The velocity contours show that at planes P1 and P2 located  $0.5$  mm and  $0.3$  mm, respectively, from the axial filament, the velocities are relatively higher than at plane P3 which is closest to the axial filament. The flow patterns obtained for type 2DC1-30 indicate that the velocities in the region I are lower when compared to planes P1 and P2 but are higher when compared to the values at plane P3. The temperature contours in Fig. 6b, d, f, h do not show significant differences due to high heat transfer rates near the membrane wall. A small region marked as III in Fig. 6f close to the membrane is an exception where temperature gradients are smaller due to temperature polarization.

The variation of shear stress, temperature and temperature polarization index in the  $x$ -direction are shown in Fig. 7 for the same three- and two-dimensional geometries. The values are obtained at the three horizontal planes at distances

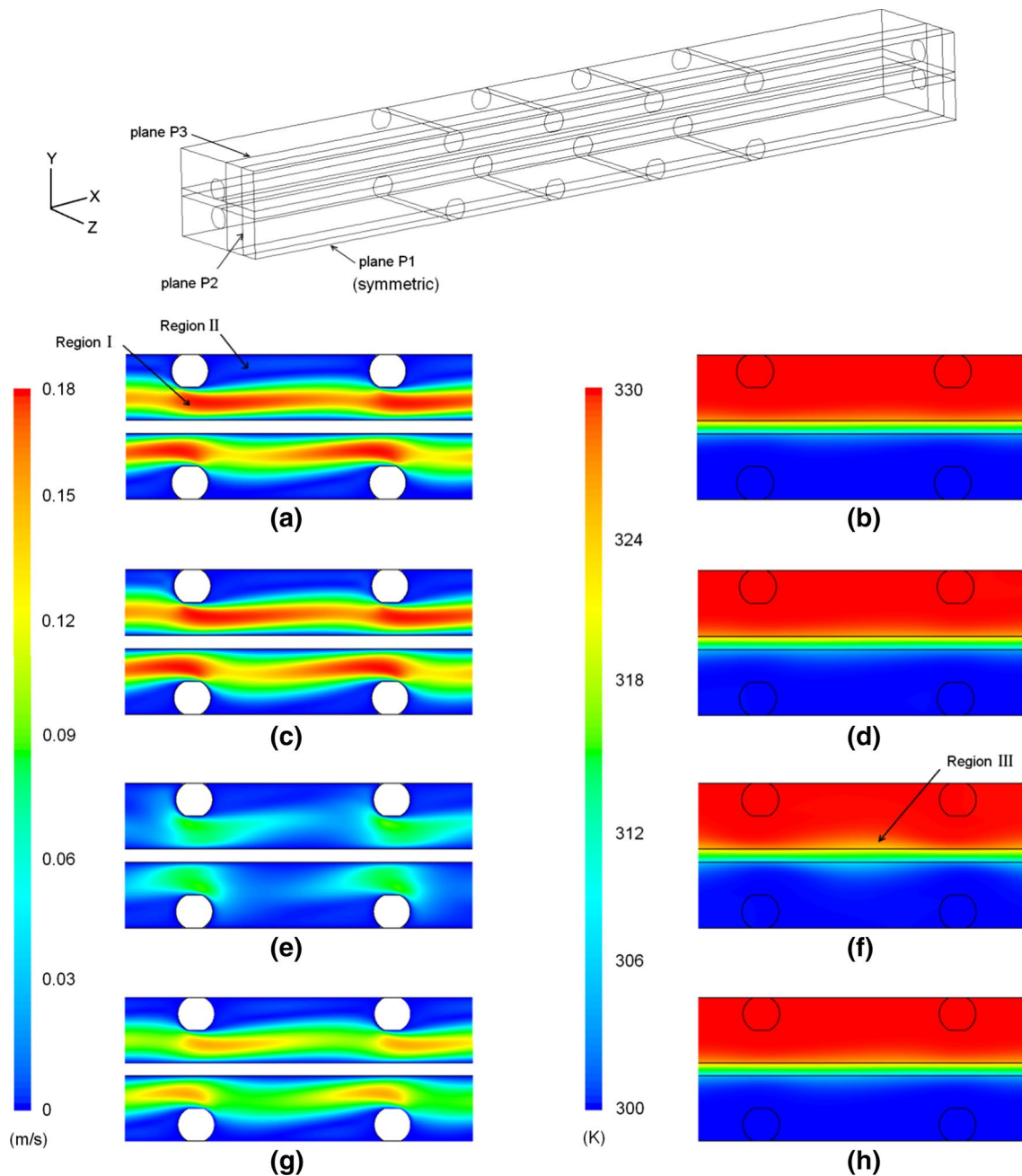


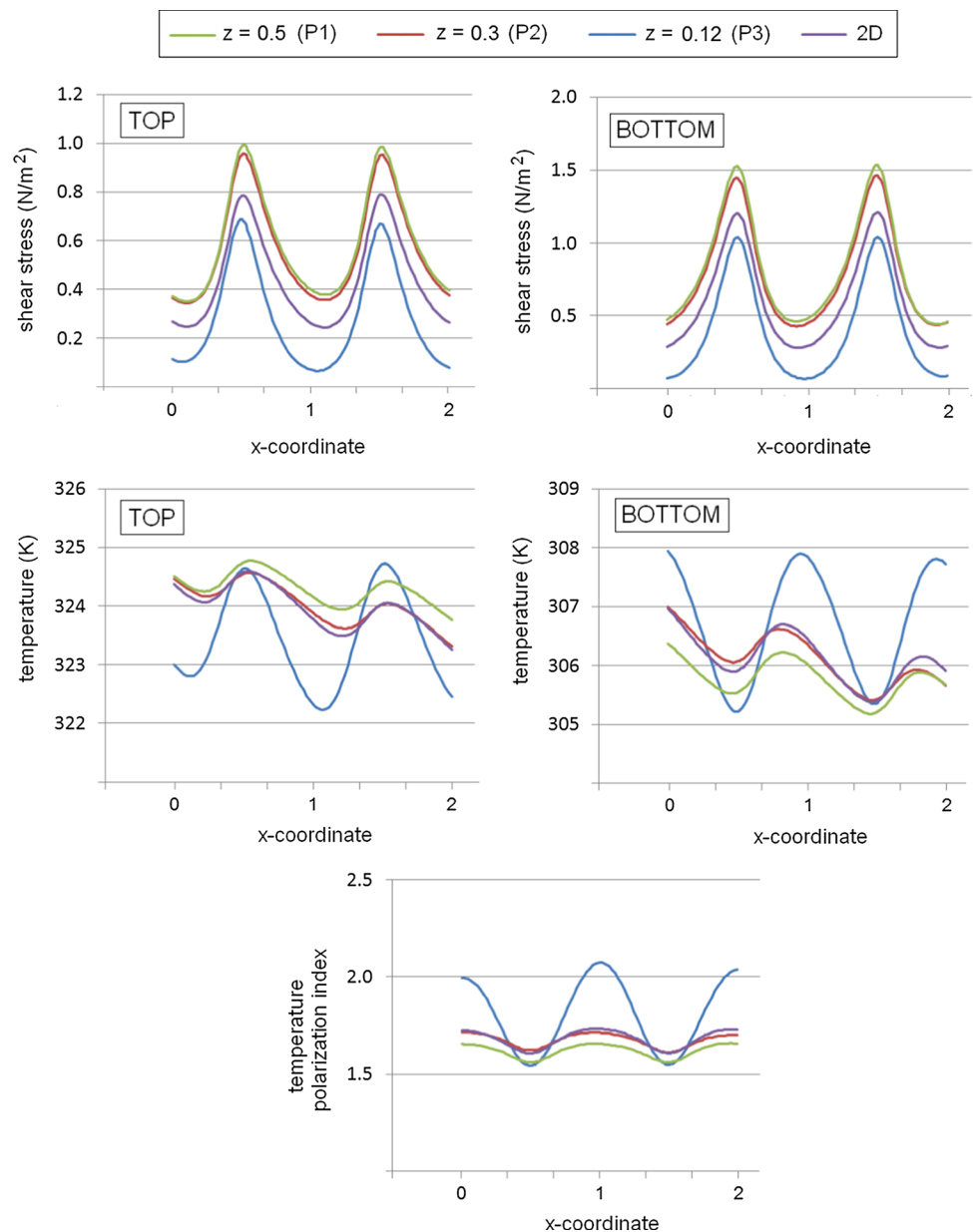
**Fig. 6** Velocity and temperature profiles in 3DC1-30 **a, b** P1; **c, d** P2; **e, f** P3 and **g, h** 2DC1-30

of 0.12, 0.3 and 0.5 from the axial filament as well as on the top and bottom membrane surfaces. The transverse filaments in Fig. 7 are located at  $x=0.5$  and  $1.5$  ( $x$  is non-dimensionalized by spacing  $l_m$ ). Higher shear stress is desirable to reduce fouling at the membrane surface. Additionally, a higher temperature difference is required on the two sides of the membrane surface to decrease temperature polarization and increase vapor permeation through the membrane. It was observed in velocity contours in Fig. 6 that the velocity increased in the region I due to the reduced area available

for fluid to move between membrane surface and transverse filament. An increase in velocity magnitude increases velocity gradients in this region and wall shear stresses at the filament and at the membrane. At the membrane surfaces (passing through  $z=0.12, 0.3$  and  $0.5$ ) for 3-d geometry and at the membrane surface of 2-d geometry, maximum values of shear stress are thus seen at the top and the bottom membrane surfaces at  $x=0.5$  and  $1.5$  which are positions directly above or below the filament. When compared with 2-d simulations, the local shear stress for 3-d simulations is found to



**Fig. 7** Shear stress, temperature and temperature polarization index in a 3-d geometry (3DC1-30) at three planes and a 2-d geometry (2DC1-30)



be lower at  $z=0.12$  but higher for  $z=0.3$  and  $z=0.5$ . The temperature plots in Fig. 7 indicate that the temperature at the top membrane side is higher at the same position where shear stress is higher. Similarly, the temperature at the bottom membrane side is lower where shear stress is higher. The higher temperature at the top or lower temperature at the bottom surface lowers the  $\phi$ .

The temperature line plot shows that the temperature variation is relatively small at locations  $z=0.3$  and  $z=0.5$  in the 2-d geometry. The temperature range is between 323–325 K and 305–307 K for the top and the bottom membrane surfaces, respectively. At location  $z=0.12$ , the temperature range is slightly bigger and is between 322–325 K and 305–308 K for the top and bottom membrane surfaces,

respectively. These differences create different  $\phi$  patterns, and it is found that the  $\phi$  values obtained from 2-d simulations are nearly the same as those obtained for locations  $z=0.3$  and  $z=0.5$  from the 3-d modeling. However, the  $\phi$  obtained with 2-d modeling is different from the one obtained at  $z=0.12$  due to strong three-dimensional effects at this plane. Figures 6 and 7 are specific for spacer orientations 3DC1-30 and 2DC1-30, but similar results are found for other in-line and staggered orientations of Table 1.

The average values of shear stress and its standard deviation (relative to average value) are plotted in Fig. 8 which shows that the average shear stress increases sharply as the inlet velocity increases. For the different orientations considered in this study, the average shear rate curve obtained

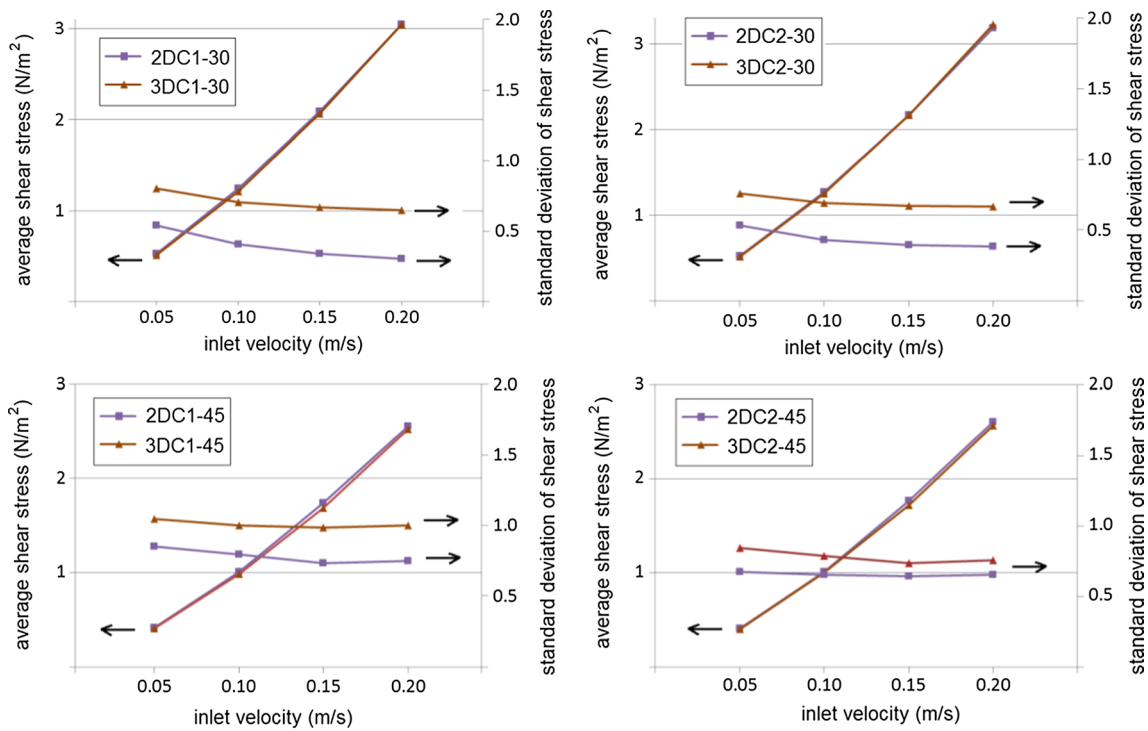


Fig. 8 Average shear stress and its standard deviation as a function of inlet velocity

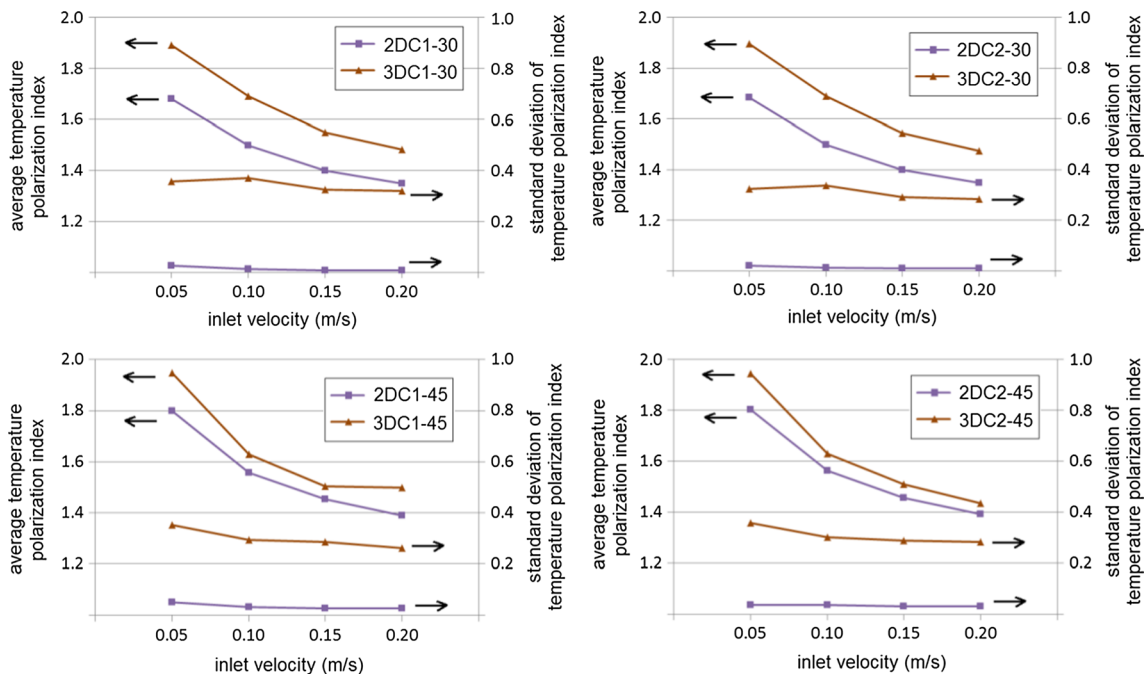


Fig. 9 Average temperature polarization index and its standard deviation as a function of inlet velocity

from 2-d simulations overlap the curve obtained from the 3-d simulations indicating that the 2-d model suffices to predict the average shear stress values accurately. The

reason being that in 3-d simulations, at  $z=0.3$  and  $z=0.5$ , the shear stress is higher while it is lower near the axial filament at  $z=0.12$  when compared with the 2-d model. This

**Table 2** Variation (slope) of shear stress and temperature polarization with velocity obtained using linear regression method

Spacer type	$\Delta\tau_{av}/\Delta u_{av}$	$\Delta\tau_{sd}/\Delta u_{av}$	$\Delta\phi_{av}/\Delta u_{av}$	$\Delta\phi_{sd}/\Delta u_{av}$
2DC1-30	16.79	-1.54	-2.19	-0.12
3DC1-30	16.93	-0.98	-2.74	-0.32
2DC2-30	17.74	-0.96	-2.22	-0.07
3DC2-30	18.1	-0.62	-2.81	-0.34
2DC1-45	14.33	-0.73	-2.67	-0.16
3DC1-45	14.12	-0.32	-2.95	-0.55
2DC2-45	14.71	-0.62	-2.69	-0.034
3DC2-45	14.47	-0.22	-3.3	-0.48

approximately leads to equal average shear stress values in the two approaches. However, in the 3-d approach, the standard deviation is about 10–40% higher than the 2-d results. This is because the 2-d analysis calculates local wall shear stress variation only in the *x*-direction. The changes in flow properties are not calculated/considered in the *z*-direction. In the 3-d approach, the variation of local shear stresses is studied in the *x*-direction as well as in the *z*-direction as was shown in Fig. 7. Since the shear stress considerably reduces in the *z*-direction (e.g., at *z*=0.12), the standard deviation is found higher in the 3-d case.

The average and relative standard deviation of local temperature polarization index ( $\phi$ ) are also determined and the plots versus velocity are shown in Fig. 9. Due to the analogy of momentum and heat transfer, it can be expected that heat transfer will increase with inlet velocity or Reynolds

number. In all cases, it is thus observed that as the inlet velocity increases, the average temperature polarization index decreases indicating higher heat transfer rates at higher inlet velocity. Increased inlet velocity also results in more uniform temperature distribution at the membrane surface. The plots of the standard deviation of  $\phi$  versus velocity, hence, show a decreasing trend for most of the cases. A noticeable difference is observed between the 2-d and the 3-d results. From the comparison, it is seen that  $\phi_{av}$  is relatively higher and  $\phi_{sd}$  is much higher in 3-d geometries. The higher values of  $\phi_{av}$  are due to the formation of a region of significant temperature polarization in 3-d simulations close to the axial filament (such as seen in Fig. 7). The effect of axial filament cannot be examined using the 2-d simulations. A lower average  $\phi$  value using 2-d analysis indicates that the heat transfer rates are over-predicted. This particular finding for heat transfer in an MD process is different from the results of the spacer-filled ultrafiltration process in which lower mass transfer rates in 2-d simulations were reported [29]. The difference between 2-d and 3-d in terms of  $\phi_{av}$  is found more in spacers which have a spacing of 3 mm. This means three-dimensional effects become more significant when filament spacing is lower. A decrease in spacing increases the size of the stagnant region near the axial filament in which local temperature polarization indices are higher.

To better understand the trend or rate of change of various parameters, the linear regression technique is a suitable approach [30, 31]. Using this technique, the increase or decrease of shear stress and temperature polarization

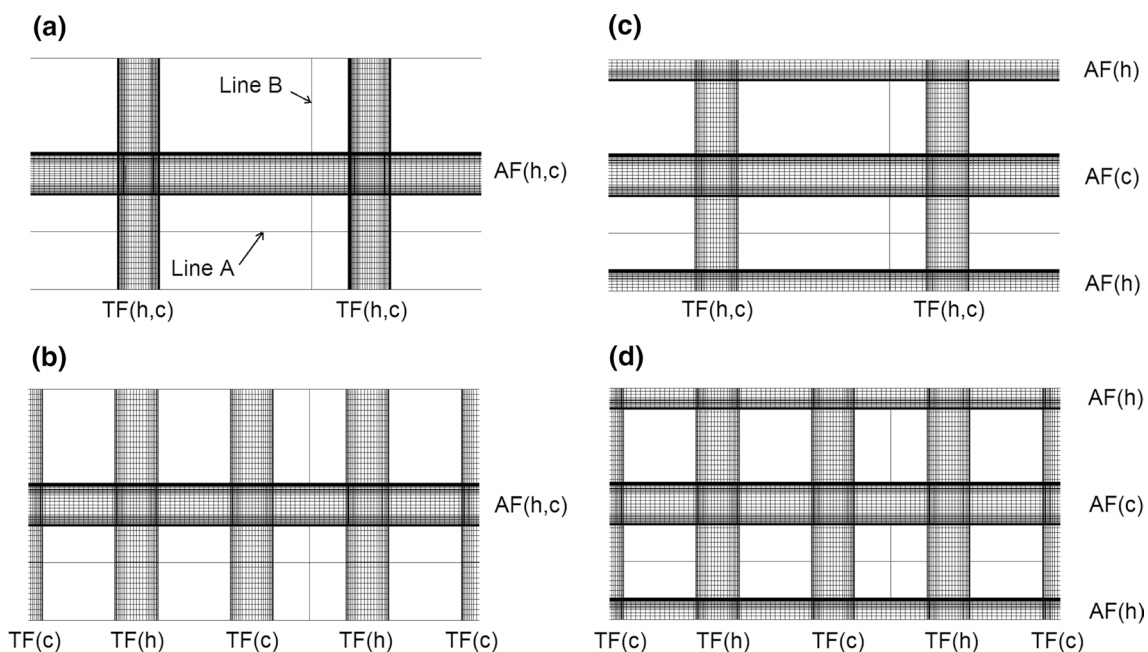


**Fig. 10** Lines in axial and transverse directions for the four spacer orientations

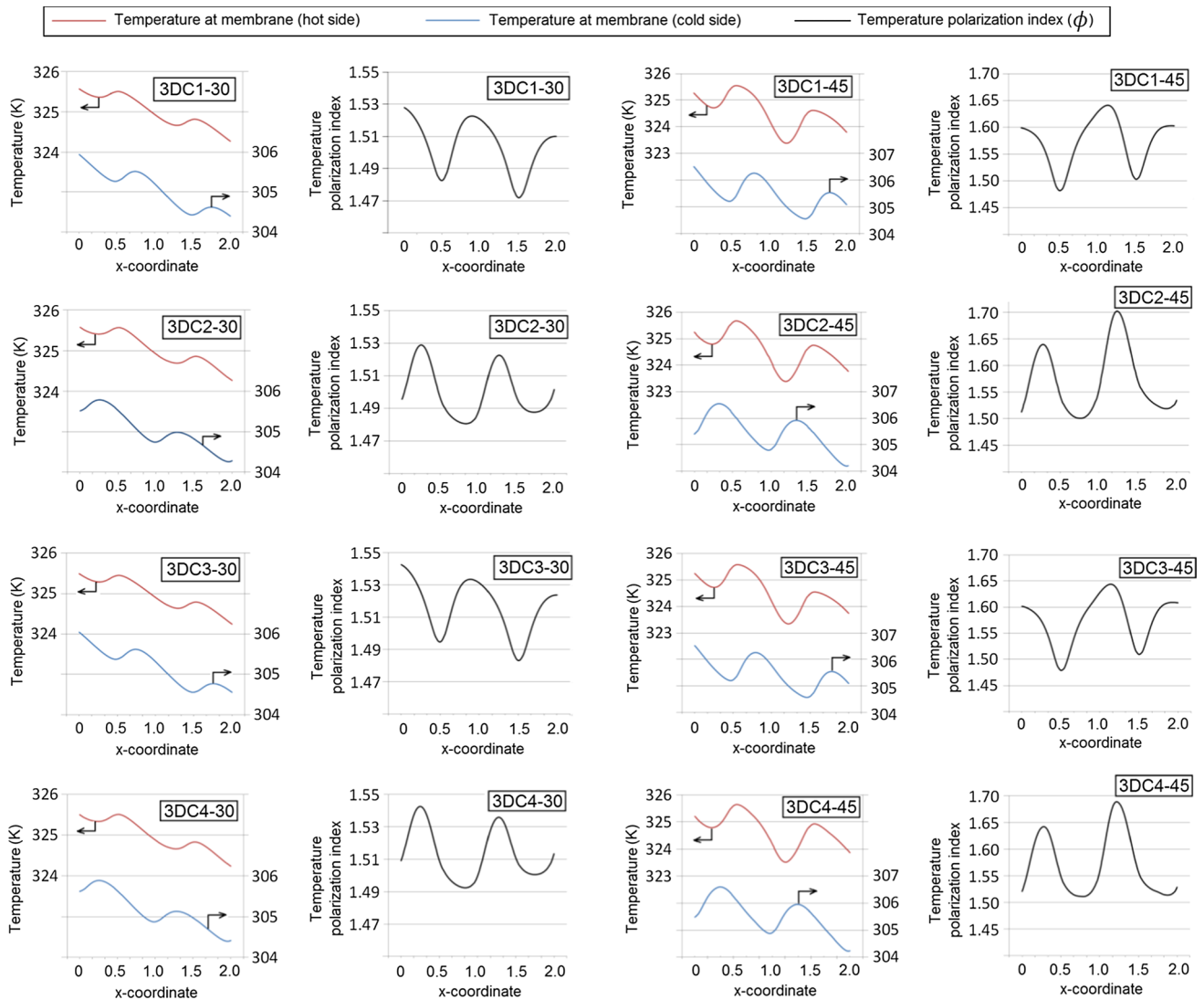


**Fig. 11** Variation of temperature and temperature polarization index in  $x$ -direction

(average and standard deviation values) with velocity, i.e., the slopes of  $\tau_{av}$ ,  $\tau_{sd}$ ,  $\phi_{av}$  and  $\phi_{sd}$  are determined and the values are given in Table 2. The comparison of 2-d and 3-d average shear stress ( $\tau_{av}$ ) slopes indicates good agreement since the differences for considered arrangements are within 2%. The standard deviations of shear stress reduce with velocity in both 2-d and 3-d geometries, but the reduction is relatively more in 2-d ones. This means that shear stress becomes more uniform when velocity is increased. The average temperature polarization indices decline due to an increase in velocity. The changes in standard deviations of temperature polarization index with velocity ( $\Delta\phi_{sd}/\Delta u_{av}$ ) are negligible in 2-d geometries since slopes are almost zero. In 3-d results, the  $\Delta\phi_{sd}/\Delta u_{av}$  values show a decreasing trend and the rate of decrease is more in spacers with relatively large spacing. This shows

that local temperatures become more uniform due to an increase in velocity.

In the 2-d modeling, the effect of staggering can be studied only for the transverse filaments since the axial filaments are not modeled. In the actual 3-d model, four possibilities exist as described in Table 1. Since the feed and permeate channels are separate and permeation through the membrane being small is ignored, changing the orientation does not affect the shear rates at the membrane surface. The four orientations are therefore studied only for the variation of temperature and the  $\phi$  while shear rates are not calculated. To study the variation of  $\phi$ , two imaginary lines A and B are drawn at distances  $x/4$  and  $z/4$  from the transverse and axial filaments, respectively, as shown in Fig. 10. Variation of temperature on top and bottom membrane walls ( $T_{hm}$  and  $T_{cm}$ ) and  $\phi$  in the  $x$ -direction (along the  $z = x/4$  plane)

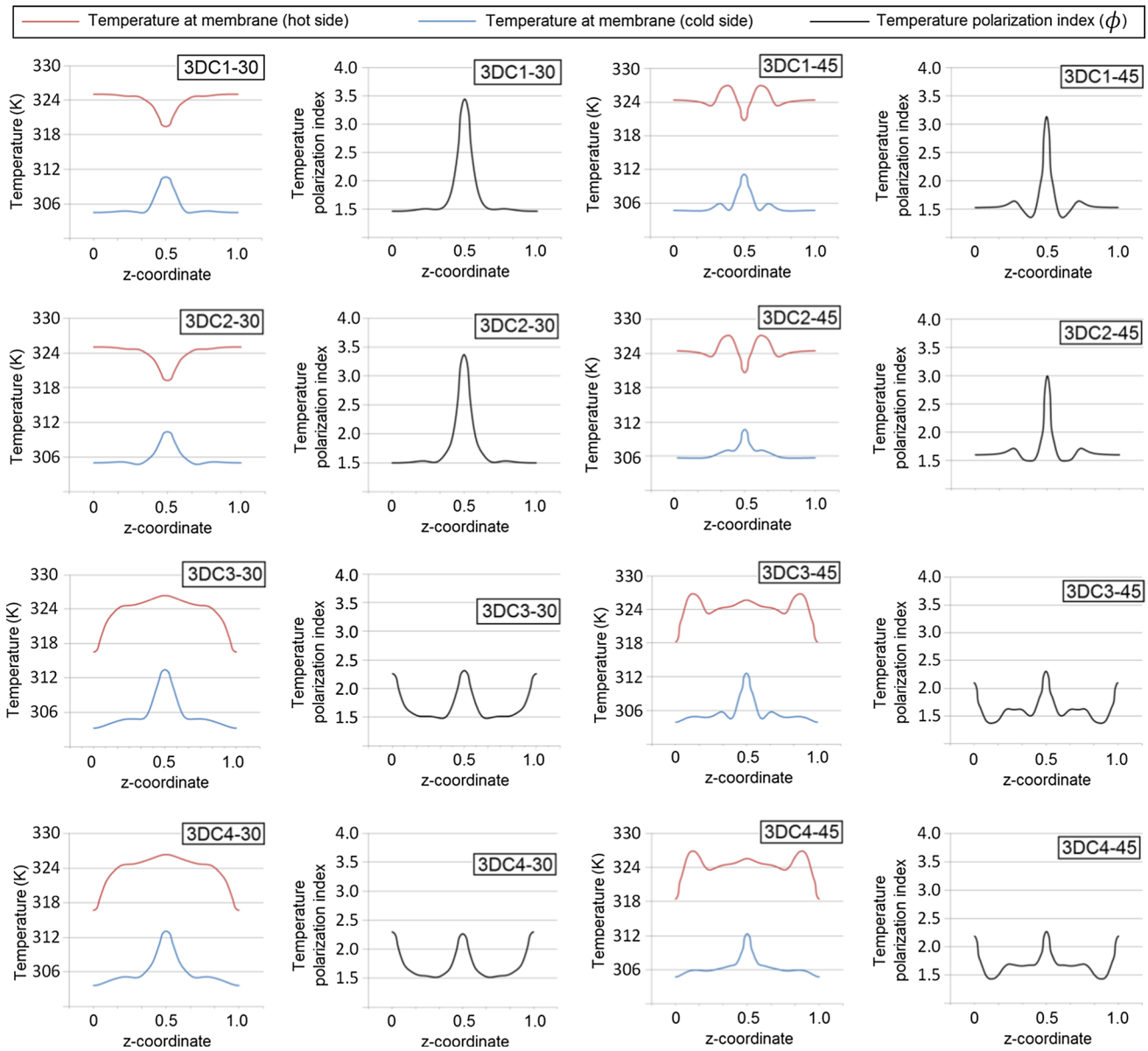


Fig. 12 Variation of temperature and temperature polarization index in  $z$ -direction

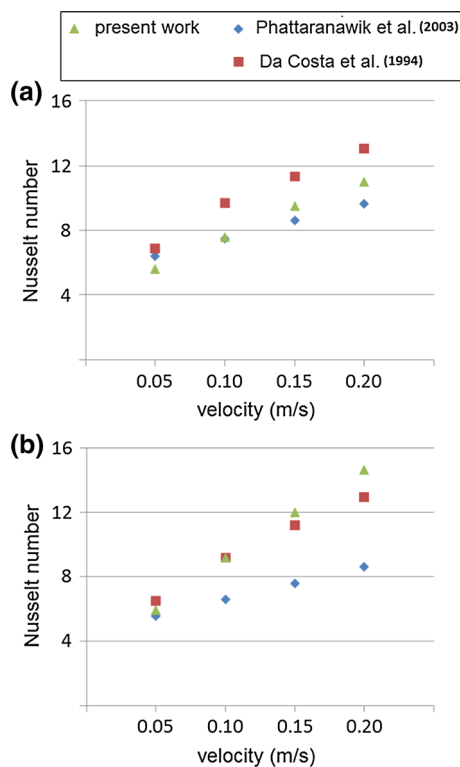
is calculated for an inlet velocity of 0.1 m/s and shown in Fig. 11. When inlet velocities are small, as seen for the case ( $u_{av} = 0.05$  m/s), the local temperatures on hot feed side in 3DC1-30 are higher at  $x = 0.5$  and  $1.5$ . At the same  $x$  location, temperature values on the cold side are lower. This reduces the  $\phi$  at these locations. In 3DC3-30, 3DC1-45 and 3DC3-45 (the geometries with in-line transverse filaments), the minimum  $\phi$  values are again found at  $x = 0.5$  and  $x = 1.5$ . For other orientations that contain staggered transverse filaments, the minimum is found between  $x = 0.8-0.9$  and  $x = 1.8-1.9$ . The  $\phi$  for geometries with 3 mm spacing varies

from 1.47 to 1.54, while for 4.5 mm spacing, the range is relatively wider and is between 1.5 and 1.7.

The membrane surface temperatures in the feed ( $T_{hm}$ ) and permeate ( $T_{cm}$ ) channels as well as  $\phi$ , are determined in the  $z$ -direction along the imaginary plane at  $x = z/4$ . It is observed that at  $z = 0.5$ , (the location of axial filament in both channels in the 3DC1 and 3DC2 configurations),  $T_{hm}$  is minimum while  $T_{cm}$  is maximum as shown in Fig. 12.

**Table 3** Average value and standard deviation of temperature polarization index as a function of inlet velocity

Spacer type	Temperature polarization index	Inlet velocity (m/s)			
		0.05	0.10	0.15	0.20
3DC1-30	$\Phi_{av}$	1.892	1.692	1.550	1.483
	$\Phi_{sd}$	0.358	0.371	0.325	0.320
3DC2-30	$\Phi_{av}$	1.896	1.689	1.545	1.475
	$\Phi_{sd}$	0.325	0.337	0.292	0.284
3DC3-30	$\Phi_{av}$	1.887	1.686	1.547	1.478
	$\Phi_{sd}$	0.164	0.174	0.156	0.154
3DC4-30	$\Phi_{av}$	1.895	1.687	1.545	1.477
	$\Phi_{sd}$	0.163	0.175	0.157	0.156
3DC1-45	$\Phi_{av}$	1.949	1.630	1.505	1.499
	$\Phi_{sd}$	0.351	0.293	0.285	0.263
3DC2-45	$\Phi_{av}$	1.945	1.631	1.511	1.435
	$\Phi_{sd}$	0.358	0.302	0.289	0.282
3DC3-45	$\Phi_{av}$	1.942	1.629	1.504	1.427
	$\Phi_{sd}$	0.187	0.170	0.168	0.164
3DC4-45	$\Phi_{av}$	1.943	1.639	1.517	1.441
	$\Phi_{sd}$	0.195	0.182	0.176	0.176

**Fig. 13** Comparison of Nusselt numbers obtained from CFD in a) 3DC1-30 and b) 3DC1-45 orientations with experiments

Significant temperature polarization thus occurs at this location, and  $\phi$  is between 3 and 3.5. In the 3DC3 and 3DC4 configurations, the region where  $T_{cm}$  is high  $T_{hm}$  is

also high and vice versa. This leads to relatively moderate values of  $\phi$  ( $\phi \approx 2.3$ ). However, for the 3DC4 case, three different maxima are clearly visible at three different  $z$  locations, i.e., at  $z = 0$ ,  $z = 0.5$  and  $z = 1.0$ . The effect of increasing the spacing from 3 to 4.5 mm is seen for some configurations. For example, the  $\phi$  value in 3DC1-30 varies from 1.5 to 3.5, while in 3DC1-45 the index range is 1.4–3.1.

Figures 11 and 12 are for an inlet velocity of 0.1 m/s. For other velocities, the numerical values of  $\phi$  are different but the pattern of variation is identical. The average and standard deviation of  $\phi$  at other velocities are summarized in Table 3. The results show that the average temperature polarization index ( $\phi_{av}$ ) may decrease up to 25%, as the inlet velocity is increased from 0.05 to 0.2 m/s. It is further noticed that at smaller velocities, the spacers with smaller filament spacing are better due to lower  $\phi$  value, whereas, for higher velocities, the spacers with larger filament spacing are found to be better. The average  $\phi$  values are generally found independent of the type of configuration as the difference is only 1–2%. Overall, the lowest  $\phi_{av}$  is found in orientation 3DC3-45 which has staggered axial filaments with a spacing of 4.5 mm.

As seen in Table 3, the standard deviation ( $\phi_{sd}$ ) decreases with the increase in inlet velocity for most of the cases. The  $\phi_{sd}$  values of in-line and staggered transverse filament configurations indicate that for smaller spacing (3 mm), the configuration 3DC2-30 with staggered transverse filaments has a better  $\phi$  distribution as compared to the in-line 3DC1-30 configuration. When the spacing is larger (4.5 mm), the difference between these two configurations is small and little difference is seen in  $\phi_{sd}$  values of 3DC1-45 and 3DC2-45 except when the velocity is 0.2 m/s. The difference between the configurations that have in-line axial filaments (3DC1 and 3DC2) and the configurations with staggered axial filaments (3DC3 and 3DC4) is found to be significant. The configurations with staggered axial filaments are found to be more suitable for MD applications as they result in low  $\phi_{sd}$  values. This gives uniform permeate mass flow through various portions of the membrane.

The present CFD results are compared with the experimental results available in the literature. Since there is not a significant variation in the average temperature polarization index or average heat transfer coefficient for the various geometric configurations considered in this work, only configurations 3DC1-30 and 3DC1-45 are chosen for comparison. Nusselt numbers are computed and compared with published experimental correlations provided as Eqs. (3) and (4) in this paper. The comparison is shown in Fig. 13; it can be seen that at smaller velocities the difference in Nusselt numbers is less than 15% but at higher velocities, the difference becomes larger. Considering the wide variation of reported experimental results in the literature, the difference

in Nusselt number values presented in this paper with those of Phattaranawik et al. [5] and Da Costa et al. [24] is found to be reasonable and within acceptable limits.

## 4 Conclusions

In this paper, CFD simulations for several feed spacer orientations in MD modules are presented. Shear stress, temperature polarization index and Nusselt numbers for these different orientations are computed and comparison is made between 2-d and 3-d results. The average values of shear stress are found to be equal in both 2-d and 3-d approaches. However, the average temperature polarization index and standard deviation of both parameters determined from 2-d modeling do not completely match the 3-d results. The reason being that in the 2-d analysis, only the effect of transverse filaments is considered while the effect of axial filaments touching the membrane is ignored. The axial filaments create stagnant zones near the membrane surface where shear stress is small and temperature polarization is high. Due to the presence of these zones, the local shear stress and the temperature polarization index becomes non-uniform as indicated by the increased standard deviation. The effect of inlet velocity and filament spacing is also studied for several spacer configurations. A minimum value of the average temperature polarization index and its standard deviation is achieved for the configuration that has staggered axial filaments and larger spacing. Lastly, the computed Nusselt numbers from this study are found to be in reasonable agreement with the ones reported in the literature.

**Acknowledgements** The financial support provided by the Deanship of Academic Research at Al Imam Mohammad Ibn Saud Islamic University vide Research Grant 321402 is deeply appreciated and duly acknowledged.

## References

- Shakaib, M.; Hasani, S.M.F.; Ahmed, I.; Yunus, R.M.: A CFD study on the effect of spacer orientation on temperature polarization in membrane distillation modules. *Desalination* **284**, 332–340 (2012)
- Gonzalez, D.; Amigo, J.; Suarez, F.: Membrane distillation-Perspectives for sustainable and improved desalination. *Renew. Sustain. Energy Rev.* **80**, 238–259 (2017)
- Shirazi, M.M.A.; Kargari, A.; Ismail, A.F.; Matsuura, T.: Computational Fluid Dynamic (CFD) opportunities applied to the membrane distillation process-State of the art and perspectives. *Desalination* **377**, 73–90 (2016)
- Phattaranawik, J.; Jiratananon, R.; Fane, A.G.; Halim, C.: Mass flux enhancement using spacer filled channel in direct contact membrane distillation. *J. Membr. Sci.* **187**, 193–201 (2001)
- Phattaranawik, J.; Jiratananon, R.; Fane, A.G.: Effects of net-type spacers on heat and mass transfer in direct contact membrane distillation and comparison with ultrafiltration studies. *J. Membr. Sci.* **217**, 193–206 (2003)
- Martínez, L.; Vázquez-González, M.I.; Florido-Díaz, F.J.: Study of membrane distillation using channel spacers. *J. Membr. Sci.* **144**, 45–56 (1998)
- Martínez, L.; Rodríguez-Maroto, J.M.: Characterization of membrane distillation modules and analysis of mass flux enhancement by channel spacers. *J. Membr. Sci.* **274**, 123–137 (2006)
- Martínez, L.; Vázquez-González, M.I.: Temperature and concentration polarization in membrane distillation in aqueous salt solutions. *J. Membr. Sci.* **156**, 265–273 (1999)
- Chernyshov, M.N.; Meindersma, G.W.; de Haan, A.B.: Comparison of spacers for temperature polarization reduction in air gap membrane distillation. *Desalination* **183**, 363–374 (2005)
- Xu, Z.; Pan, Y.; Yu, Y.: CFD simulation on membrane distillation of NaCl solution. *Front. Chem. Eng. China* **3**, 293–297 (2009)
- Alklaibi, A.M.; Lior, N.: Flow modification spacers in membrane distillation (MD) channels. *Proc. IDA World Congress, Gran Canaria* (2007)
- Cipollina, A.; Di Miceli, A.; Koschikowski, J.; Micale, G.; Rizzuti, L.: CFD simulation of a membrane distillation module channel. *Desalination Water Treat* **6**, 177–183 (2009)
- Cipollina, A.; Micale, G.; Rizzuti, L.: Membrane distillation heat transfer enhancement by CFD analysis of internal module geometry. *Desalination Water Treat* **25**, 195–209 (2011)
- Jangwon, S.; Kim, Y.M.; Kim, J.H.: Spacer optimization strategy for direct contact membrane distillation—shapes, configurations, diameters, and numbers of spacer filaments. *Desalination* **417**, 9–18 (2017)
- Al-Sharif, S.; Albeirutty, M.; Cipollina, A.; Micale, G.: Modeling flow and heat transfer in spacer-filled membrane distillation channels using open source CFD code. *Desalination* **311**, 103–112 (2013)
- Yu, H.; Yang, X.; Wang, R.; Fane, A.G.: Analysis of heat and mass transfer by CFD for performance enhancement in direct contact membrane distillation. *J. Membr. Sci.* **405–406**, 38–47 (2012)
- Chang, H.; Hsu, J.A.; Chang, C.L.; Ho, C.D.: CFD study of heat transfer enhanced membrane distillation using spacer filled channels. *Energy Procedia* **75**, 3213–3219 (2015)
- Katsandri, A.: A theoretical analysis of a spacer filled flat plate membrane distillation modules using CFD-Part II: temperature polarization analysis. *Desalination* **408**, 166–180 (2017)
- Katsandri, A.: An experimental and CFD theoretical study of enhancing mass flux in flat plate direct contact membrane distillation. PhD thesis, Department of Construction Management and Engineering, Reading University, Reading UK (2011)
- Shakaib, M.; Hasani, S.M.F.; Haque, M.E.; Ahmed, I.; Yunus, R.M.: A CFD study of heat transfer through spacer channels of membrane distillation modules. *Desalination Water Treat.* **51**, 3662–3674 (2013)
- Neal, P.R.; Li, H.; Fane, A.G.; Wiley, D.E.: The effect of filament orientation on critical flux and particle deposition in spacer-filled channels. *J. Membr. Sci.* **214**, 165–178 (2003)
- Radu, A.I.; van Steen, M.S.H.; Vrouwenvelder, J.S.; van Loosdrecht, M.C.M.; Picoreanu, C.: Spacer geometry and particle deposition in spiral wound membrane feed channels. *Water Res.* **64**, 160–176 (2014)
- Santos, J.L.C.; Geraldés, V.; Velizarov, S.; Crespo, J.G.: Investigation of flow patterns and mass transfer in membrane module channels filled with flow-aligned spacers using computational fluid dynamics (CFD). *J. Membr. Sci.* **305**, 103–117 (2007)
- Da Costa, A.R.; Fane, A.G.; Wiley, D.E.: Spacer characterization and pressure drop modeling in spacer-filled channels. *J. Membr. Sci.* **87**, 79–98 (1994)



25. Shakaib, M.; Ahmed, I.; Yunus, R.M.: Effect of permeation velocity on flow behavior and pressure drop in feed channels of membranes. In: Proceedings of ACSSSR Conference on Scientific and Social Science Research, Penang (2011)
26. Lawson, K.W.; Lloyd, D.R.: Membrane distillation. *J. Membr. Sci.* **124**, 1–25 (1997)
27. Ansys Fluent 12 Users' Manual, Ansys Inc. (2012)
28. Versteeg, H.K.; Malalasekera, W.: An Introduction to Computational Fluid Dynamics: The Finite Volume Method. Longman, Harlow (1996)
29. Fimbres-Weihs, G.A.; Wiley, D.E.: Numerical study of mass transfer in three-dimensional spacer-filled narrow channels with steady flow. *J. Membr. Sci.* **306**, 228–243 (2007)
30. Shah, N.A.; Animasaun, I.L.; Ibraheem, R.O.; Babatunde, H.A.; Sandeep, N.; Pop, I.: Scrutinization of the effects of Grashof number on the flow of different fluids driven by convection over various surfaces. *J. Mol. Liquids* **249**, 980–990 (2018)
31. Animasaun, I.L.; Koriko, O.K.; Adegbe, K.S.; Babatunde, H.A.; Ibraheem, R.O.; Sandeep, N.; Mahanthesh, B.: Comparative analysis between 36 nm and 47 nm alumina–water nanofluid flows in the presence of Hall effect. *J. Therm. Anal. Calorim.* **135**(2), 873–886 (2018)

